AGU PUBLICATIONS

JGR

Journal of Geophysical Research: Space Physics

RESEARCH ARTICLE

10.1002/2016JA023694

Special Section:
Magnetospheric Multiscale (MMS) mission results throughout the first primary mission phase

Key Points:
- The energetic ions observed in the upstream and downstream region of the bow shock originated in the magnetosphere
- Magnetospheric energetic ions gradient drifted out of the nearby quasi-parallel foreshock and into the quasi-perpendicular bow shock region
- Inverse dispersions can be caused by the IMF orientation changes, from quasi-perpendicular to (nearly) perpendicular local bow shock

Correspondence to:
S. H. Lee,
sun.h.lee@nasa.gov

Citation:
Lee, S. H., et al. (2017), MMS observation of inverse energy dispersion in shock drift accelerated ions, *J. Geophys. Res. Space Physics*, *122*, 3232–3246, doi:10.1002/2016JA023694.

Received 14 NOV 2016
Accepted 28 FEB 2017
Accepted article online 9 MAR 2017
Published online 16 MAR 2017

MMS observation of inverse energy dispersion in shock drift accelerated ions

S. H. Lee[1], D. G. Sibeck[1], K.-J. Hwang[1,2], Y. Wang[3], M. V. D. Silveira[1], C. Chu[4], B. H. Mauk[5], I. J. Cohen[5], G. C. Ho[5], G. M. Mason[5], R. E. Gold[5], J. L. Burch[6], B. L. Giles[1], R. B. Torbert[7], C. T. Russell[8], and H. Wei[8]

[1]NASA Goddard Space Flight Center, Greenbelt, Maryland, USA, [2]Goddard Planetary and Heliophysics Institute, University of Maryland, Baltimore County, Baltimore, Maryland, USA, [3]Institute of Space Physics and Applied Technology School of Earth and Space Sciences, Peking University, Beijing, China, [4]Physics Department and Geophysical Institute, University of Alaska Fairbanks, Fairbanks, Alaska, USA, [5]The Johns Hopkins University Applied Physics Laboratory, Laurel, Maryland, USA, [6]Southwest Research Institute, San Antonio, Texas, USA, [7]Department of Physics and Space Science Center, University of New Hampshire, Durham, New Hampshire, USA, [8]Institute of Geophysics and Planetary Physics, University of California, Los Angeles, California, USA

Abstract The four Magnetospheric Multiscale (MMS) spacecraft observed a ~1 min burst of energetic ions (50–1000 keV) in the region upstream from the subsolar quasi-perpendicular bow shock on 6 December 2015. The composition, flux levels, and spectral indices of these energetic protons, helium, and oxygen ions greatly resemble those seen in the outer magnetosphere earlier while MMS crossed the magnetopause and differ significantly from those simultaneously observed far upstream by Advanced Composition Explorer (ACE). However, the event cannot be explained solely in terms of leakage from the magnetosphere. The strongly southward orientation of the interplanetary magnetic field (IMF) lines at the time of the event precludes any connection to the magnetosphere. This point is confirmed by the presence of energetic electrons, known to occur on magnetic field lines that graze the bow shock rather than connect to the magnetosphere. We suggest that the ions gradient drifted out of the nearby quasi-parallel foreshock and into the quasi-perpendicular bow shock. Each of the ion species exhibited an inverse energy dispersion. As predicted by models for shock drift acceleration, the energies of the ions increased as θ_{Bn}, the angle between the IMF and the shock normal, increased. Finally, we note that a similar event was observed a few minutes later in the subsolar magnetosheath, indicating that such events can be swept downstream of the bow shock.

1. Introduction

Energetic particles are often observed in the vicinity of the Earth's bow shock [e.g., *Asbridge et al.*, 1968; *Lin et al.*, 1974; *Terasawa*, 1979]. These energetic particles are divided into three categories according to their origins: solar energetic particles (SEPs), high-energy particles escaping by leakage from the magnetosphere, and particles accelerated locally upstream of the bow shock by processes such as Fermi acceleration and shock drift acceleration. The origin of the solar energetic particles (SEPs) is thought to be solar flares, coronal mass ejections (CMEs), and interplanetary shocks [e.g., *Kahler*, 1994; *Reames et al.*, 1994]. Preaccelerated magnetospheric ions with large gyroradii can escape from the magnetosphere [e.g., *Sibeck et al.*, 1987], perhaps along reconnected magnetic field lines [e.g., *Zong et al.*, 2001; *Lee et al.*, 2016], and eventually reach the region upstream from the bow shock [e.g., *Anagnostopoulos et al.*, 1986; *Sarris et al.*, 1987; *Sibeck et al.*, 1988]. Ambient energetic particles of solar origin can be accelerated up to high energies (several MeV) by Fermi or shock drift acceleration mechanisms [e.g., *Decker*, 1988; *Giacalone*, 2004].

As described below, energy-time dispersed ion structures are often attributed to the leakage of substorm injected ion dispersions in the magnetosphere or Fermi acceleration upstream from the bow shock [*Anagnostopoulos et al.*, 2000; *Ipavich et al.*, 1981a, 1981b; *Louarn et al.*, 2003]. Normal dispersion patterns are observed when the high-energy particles are first detected. They can be explained by time-of-flight effects. Inverse dispersions, with the lower energy particles reaching the observing spacecraft before the higher-energy particles, can be interpreted as the result of temporal or spatial effects. These dispersion signatures help us to understand the behavior and temporal/spatial development of the upstream energetic particles and dynamic processes near the bow shock.

The Magnetospheric Multiscale (MMS) Energetic Ion Spectrometer (EIS) distinguishes energetic ion species, proton (~20 keV to ~1 MeV), helium (~60 keV to ~1 MeV), and oxygen ions (~130 keV to ~1 MeV) and also measures energetic electrons (~25–600 keV). EIS detected well-defined inverse dispersion event in the region upstream from the quasi-perpendicular bow shock and in the magnetosheath near a bow shock crossing. In this paper, we present a detailed description of the inverse energy dispersion events observed by MMS compared with those previously reported. We compare the energy spectra of the energetic ions for each species observed upstream and downstream from the bow shock by MMS and far upstream by Advanced Composition Explorer (ACE) in order to investigate the origin of the burst of energetic ions. We discuss how these energetic ions of magnetospheric origin can be present upstream from the quasi-perpendicular bow shock region in which the interplanetary magnetic field (IMF) is disconnected from the magnetosphere. We suggest that the ions can gradient drift out of the nearby quasi-parallel foreshock and into the quasi-perpendicular bow shock regime. We also investigate a possible new mechanism for producing the inverse dispersions in the region upstream from the quasi-perpendicular bow shock.

2. MMS Observations

In this section, we will present observations of two unusual inverse energy dispersion events, one upstream from the bow shock and the other in the magnetosheath. The four MMS spacecraft [*Burch et al.*, 2016] crossed the bow shock several times just south of the subsolar point near $(X, Y, Z)_{\mathrm{GSM}} = (11.7, 0.0, -1.0)\ R_E$ on 6 December 2015 from 07:50 UT to 08:30 UT. Figure 1 shows MMS 2 Fluxgate Magnetometer (FGM) [*Torbert et al.*, 2014; *Russell et al.*, 2014], Fast Plasma Investigation (FPI) [*Pollock et al.*, 2016], and Energetic Ion Spectrometer (EIS) [*Mauk et al.*, 2014] observations. We use the fast survey data for the magnetic field (60 ms), electron and total ion plasma moments (4 s), and energetic proton (~20 keV to ~1 MeV), helium (~60 keV to ~1 MeV), oxygen ions (~130 keV to ~1 MeV), electrons (~25–600 keV) intensities (~2.5 s), and their pitch angle distributions (~20 s). EIS does not measure helium and oxygen ion charge states.

From top to bottom, Figure 1 shows (a) the magnetic field strength and components, (b) the FPI thermal ion energy-time spectrogram, (c) the FPI thermal electron energy-time spectrogram, (d) the ion number density, (e) the three components of the FPI plasma velocity, (f) the FPI ion temperature (parallel and perpendicular to the magnetic field), and (g–l) EIS energy spectrograms and pitch angle distributions for proton, helium, and oxygen ions. All three ion species exhibit two clear inverse energy dispersion ion structures during the interval from 08:16:00 UT to 08:26:00 UT, as can be seen more readily in the expanded eight panels (Figures 1m–1v). These panels show (from the top panel) (m) the total magnetic field strength, (n) the three components of the magnetic field, (o) the FPI ion energy-time spectrogram, (p) the clock angle (= $\tan^{-1}$(IMF B_Y, IMF B_Z)), (q) the cone angle (= $\cos^{-1}$(IMF $|B_X|$ / IMF B_{tot})), (r) the theta Bn ($\theta_{\mathrm{Bn}} = \cos^{-1}$(IMF B$\cdot\hat{n}$ / IMF $\mathrm{B_{tot}}$)), and (s) energetic electron (40–100 keV), (t) proton (50–300 keV), (u) energetic helium (80–600 keV), and (v) energetic oxygen ion (150–900 keV) energy-time spectrograms. The black lines in the energetic ion energy spectrograms (Figures 1t–1v) indicate the characteristic energies, which are derived from the energy flux divided by the particle number flux. As will be discussed in greater detail below, each of the three ion species exhibits inverse energy dispersions and enhanced fluxes at higher energies in the region upstream from the quasi-perpendicular bow shock (from 08:18:10 UT to 08:19:30 UT) and in the region downstream from the shock (from 08:23:00 UT to 08:25:00 UT). This will be clearly shown in Figure 6.

The θ_{Bn} angle is that between the local bow shock normal and the upstream magnetic field. This quantity can be used to identify different types of shocks: quasi-parallel with $0° \le \theta_{\mathrm{Bn}} < 45°$ and quasi-perpendicular with $45° \le \theta_{\mathrm{Bn}} < 90°$. We determined the normal direction ($\hat{n}$ = (0.99, 0.02, −0.06)) to the local bow shock surface using the bow shock model of *Merka et al.* [2005], which only depends on the Alfvén Mach number (~8) and the dynamic pressure (~3 nPa). The IMF cone angle (Figure 1q) and θ_{Bn} (Figure 1r) are very similar since the normal direction is mostly along the X direction.

Color bars mark two different foreshock regions; the region upstream from the quasi-parallel bow shock is shaded in gray from 08:17:20 UT to 08:18:10 UT, while the region upstream from the quasi-perpendicular bow shock is shaded in blue from 08:18:10 UT to 08:19:30 UT in Figures 1m–1v. The IMF cone angle (Figure 1q) and θ_{Bn} (Figure 1r) vary substantially with time in the region upstream from the quasi-parallel bow shock. It is well known that the level of magnetic fluctuations is high in that region [e.g., *Greenstadt et al.*, 1995]. Past work indicates, and this study confirms, that energetic electrons occur on magnetic field lines that lie tangent to the bow shock [*Anderson et al.*, 1979; *Bieber and Stone*, 1982]. The energetic electron observations provide

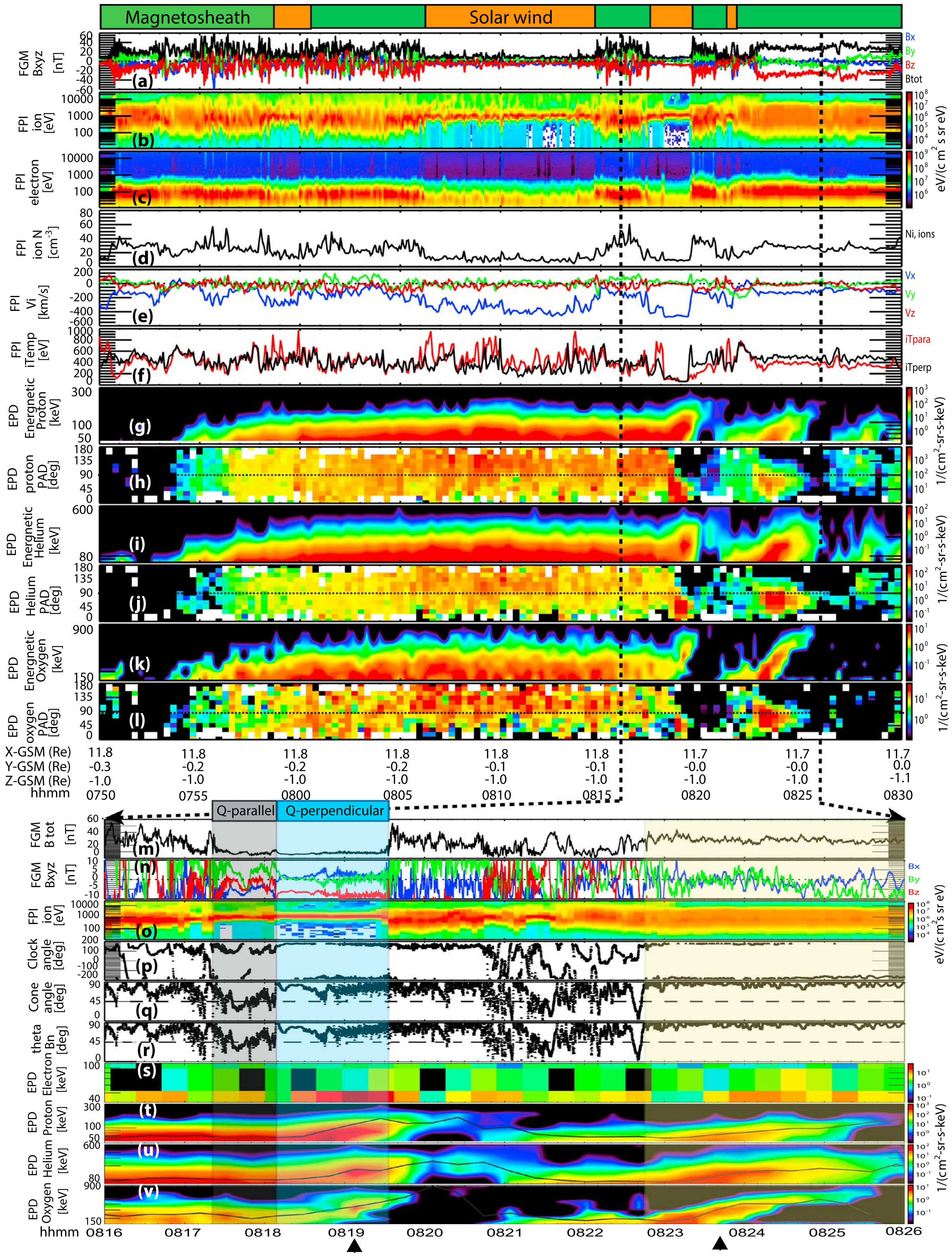

Figure 1. MMS 2 observation of the event (6 December 2015). (a) Magnetic field components in GSM coordinates and magnitude; (b) thermal ion energy flux spectrum; (c) thermal electron energy flux spectrum; (d) thermal ion density; (e) thermal plasma velocity; (f) thermal ion temperature parallel and perpendicular to the magnetic field; energy-time spectrogram from (g) 50 to 300 keV (proton), (i) 80 to 600 keV (helium), and (k) 150 to 900 keV (oxygen ions) measured by EIS; and (h, j, and l) their pitch angle distributions. The expanded time interval from 08:16 UT to 08:26 UT shows (m) magnetic field strength; (n) magnetic field components from −10 nT to 10 nT; (o) ion energy flux spectrum; (p) magnetic field clock angle; (q) cone angle; (r) θ_{Bn} angle; and energetic (s) electron, (t) proton, (u) helium, and (v) oxygen ions energy spectra.

strong evidence that the MMS spacecraft were on field lines tangent to the bow shock from 08:18:10 UT to 08:19:30 UT (Figure 1s).

Field lines that lie tangent to the subsolar bow shock do not connect to the Earth's magnetopause. We therefore expect that waves generated by ions energized at the bow shock should be confined to the immediate vicinity of the shock plane, by contrast to the region upstream from the quasi-parallel shock where waves and ions energized at the bow shock can proceed further upstream along the magnetic fields. As we have already noted when discussing Figures 1q and 1r, the magnetic fields upstream from the quasi-parallel bow shock (from 08:17:30 UT to 08:18:10 UT) are indeed generally far more turbulent than those upstream from the quasi-perpendicular bow shock (08:18:10 UT to 08:19:30 UT). However, there are also magnetic fluctuations in the quasi-perpendicular foreshock from 08:19:00 UT to 08:19:30 UT (Figure 1n). This suggests that the large fluxes of energetic particles seen just upstream from in the quasi-perpendicular bow shock region can also cause intense wave activity.

Inverse energy ion dispersions occurred in the region upstream from the quasi-perpendicular bow shock (shaded region in blue) from 08:18:10 UT to 08:19:30 UT and in the magnetosheath (shaded in yellow) from 08:23:00 UT to 08:25:00 UT. The characteristic energies (black lines) of the proton, helium, and oxygen ions in the first inverse dispersion increased from approximately 60 keV to 150 keV, from 90 keV to 170 keV, and from 250 keV to 450 keV, respectively. In the second inverse dispersion pattern observed in the magnetosheath near a bow shock crossing, the energies increased from ∼70 keV to ∼150 keV for proton, from ∼100 keV to ∼200 keV for helium, and from ∼240 keV to ∼570 keV for oxygen ions.

The energetic ions that exhibited the inverse dispersions in the magnetosheath downstream of the bow shock can be a population transmitted from the upstream. There are spacecraft upstream from the bow shock that might help us determine how the second inverse dispersion signature forms. However, these solar wind monitors are not close enough to the Earth and the Sun-Earth line to serve as accurate monitors. Therefore, we focus on the first inverse dispersion event since the MMS spacecraft were in the upstream region where they themselves can monitor the solar wind with 60 ms resolution magnetic field data sufficient to check the effect of the small changes in the IMF direction on the energy dispersion signature. We shall, however, briefly compare the energy spectra of ion intensities for each species in the first inverse dispersions to those in the second inverse energy dispersions.

3. Interpretation and Discussion

3.1. Source of the Energetic Ions in the Inverse Dispersion

We seek to determine the origin of the energetic ions in the inverse dispersions. There are two possible sources for the energetic ions (50 keV to 1 MeV) observed in the foreshock and in the outer magnetosheath near the bow shock: the magnetosphere or the Sun/interplanetary medium. Energetic magnetospheric particles ($\sim 10 - 10^2$ keV) are commonly observed in the magnetosheath [e.g., *Cohen et al.*, 2016] since they can escape into the magnetosheath along the reconnected magnetospheric and magnetosheath magnetic field lines [e.g., *Zong et al.*, 2001] and/or through the leakage mechanisms (e.g., finite Lamor effect) [e.g., *Sibeck et al.*, 1987]. Magnetospheric ions with large gyroradii can even leak further into the region upstream of the bow shock when the interplanetary and magnetosheath magnetic field lines connect to the magnetosphere [*Sarris et al.*, 1976; *Krimigis et al.*, 1978; *Luhmann et al.*, 1984; *Krimigis et al.*, 1986].

Seed populations of incident solar wind ions can be accelerated up to energies of approximately hundreds of keV and approximately several MeV by diffuse shock acceleration (DSA or the first-order Fermi acceleration) [e.g., *Scholer et al.*, 1980, 1992; *Ipavich et al.*, 1981b; *Eichler*, 1981; *Lee*, 1982; *Ellison*, 1985; *Ellison and Moebius*, 1987] or shock drift acceleration (SDA) [e.g., *Terasawa*, 1979; *Decker*, 1983; *Armstrong et al.*, 1985; *Burgess*, 1987]. The accelerated ions can populate the foreshock regions and be swept downstream of the bow shock. Fermi acceleration (or DSA) operates at the quasi-parallel bow shock, and it accelerates energetic ions by multiple pitch angle scattering between scattering center (e.g., waves) and/or the bow shock. Shock drift acceleration (SDA) is effective at the quasi-perpendicular shock and causes the ambient seed energetic ions to gain energy by drifting parallel to the interplanetary electric field when they enter the shock region and encounter a magnetic field strength gradient. In other words, they can be accelerated by the gradient B drift of the ions' guiding center along the induced electric field $\mathbf{E} = -\mathbf{V}_{SW} \times \mathbf{B}$, where $\mathbf{V}_{SW}$ and $\mathbf{B}$ are the solar wind velocity and the IMF, respectively. SDA energetic ions are reflected upstream and transmitted downstream from the quasi-perpendicular bow shock after energization at the shock.

Consider the direction from which the energetic ions arrive at the MMS spacecraft. Figure 2 (first row) shows a schematic model of particle motion projected in the X-Y plane. The picture illustrates how ions gyrating around the southward magnetic field with a source at the bow shock would reach MMS outside the bow shock (Figure 2a) and how they would reach MMS in the magnetosheath (Figure 2b). This model can be qualitatively used here for the rough estimation. Figure 2 (second to fourth rows) shows the 3-D polar angle versus azimuthal angle representations of energetic proton (blue), helium (green), and oxygen ion (red) distributions measured upstream from the quasi-perpendicular bow shock from 08:19:10 UT to 08:19:30 UT (left column) and in the magnetosheath downstream from the bow shock from 08:23:41UT to 08:24:00 UT (right column) as marked by the black arrowheads at the bottom of Figure 1. White color denotes the highest fluxes, and white solid lines indicate contours of constant pitch angle.

For the first inverse dispersion event observed in the region upstream of the bow shock, the maximum fluxes of all three energetic ion species (proton, helium, and oxygen ions) occurred at positive polar angles (∼30°) and negative azimuthal angles (∼−135°), i.e., these energetic ions came from the north and dawnside, which is consistent with the prediction (Figure 2a). If the energetic ions come from the subsolar bow shock, the ions would arrive from these directions for the observed southward and dawnward IMF (B_X, B_Y, B_Z)= (3, −2, −7) nT. This indicates that acceleration at the bow shock and/or escape from the magnetosheath contribute to the energetic ions population observed in the region upstream from the bow shock.

The maximum fluxes of energetic ions in the second inverse dispersion event observed in the magnetosheath occurred at positive polar angles (∼60°) and positive azimuthal angles (∼135°), i.e., ions came from the north and duskside. This is consistent with a source lying closer to the bow shock for the observed southward magnetosheath magnetic fields. This indicates that most of the these energetic ion fluxes are associated with shock-accelerated populations swept downstream. The energetic ion fluxes in the inverse dispersions from both regions upstream and downstream of the bow shock peaked at ∼45° pitch angles.

If the origin of the energetic ions observed upstream from the quasi-perpendicular bow shock is the solar wind, then the seed solar energetic ions must be directly energized via shock drift acceleration. We compared the differential intensities for each of the ion species observed by the Advanced Composition Explorer (ACE)-Electron, Proton, and Alpha Monitor (EPAM) [*Gold et al.*, 1998], the ACE-Ultra Low Energy Isotope Spectrometer (ULEIS) [*Mason et al.*, 1998], and MMS-EIS. Figure 3 shows the energy spectra of the energetic ions (purple), ^{4}He (lime), and O (orange) at ACE and of the energetic proton (blue), helium (green), and oxygen ions (red) at MMS. The differential intensities at ACE are measured over the 1 h time averaged from 07:00:00 UT to 08:00:00 UT. ACE was located at $(X, Y, Z)_{\mathrm{GSM}}$ = (241.8, 16.5, 20.3) R_E far upstream from the bow shock. The energy spectrum at MMS is representative of shock drift accelerated (SDA) ions that are measured from 08:18:30 UT to 08:19:30 UT (1 min average) upstream from the quasi-perpendicular bow shock. The intensities at ACE are very low compared to those at MMS. The energy spectrum of the solar energetic ions obtained by ACE exhibits a different slope from that of the energetic ions observed by MMS, and the ratio of alpha particle intensities to oxygen intensities at ACE (∼262.4) differs by 1 order of magnitude from that at MMS (∼22.6). This indicates that the source of the energetic particles observed by MMS in the region upstream from the quasi-perpendicular bow shock is not the ambient solar energetic ions.

Now consider the possibility that the ions are of magnetospheric origin. Figures 4a–4h present from top to bottom (a) the three components of the magnetic field, (b) ion energy spectrum, (c) electron energy spectrum, (d) ion number density, (e) ion flow components, (f) energetic proton, (g) helium, and (h) oxygen ion energy spectrum from 00:00 UT to 01:00 UT on 6 December 2015, i.e., for the time interval including the magnetopause crossing at 00:25 UT of MMS 2. Figure 4i compares the energy spectra of the energetic proton (blue), helium (green), and oxygen ions (red) intensities in the quasi-parallel region of the bow shock (dotted lines), in the inner magnetosheath (dashed line), and in the outer magnetosphere (long-dashed lines). The ion intensities in the outer magnetosphere (Msp) and in the inner magnetosheath (Msh) are 3 min averages from 00:20 UT to 00:23 UT and from 00:25 UT to 00:28 UT, respectively. The selected two time intervals are marked by the gray vertical color bars in Figures 4a–4h. The energy spectrum of ion intensities upstream from the quasi-parallel bow shock is measured for the period from 08:17:20 UT to 08:18:20 UT marked by the gray shaded region in Figure 1. The energetic ion spectra is best fit by a power law, $\mathrm{d}J/\mathrm{d}E = kE^{-\gamma} \exp(-E/E_0)$, where J is the intensity; E is kinetic energy; and k, E_0, and γ are constants [*Ellison and Ramaty*, 1985]. The flux levels, composition, and slopes (γ) of the energy spectra in each region are similar. This suggests that the energetic ions observed upstream escaped from the magnetosphere along magnetic fields that were

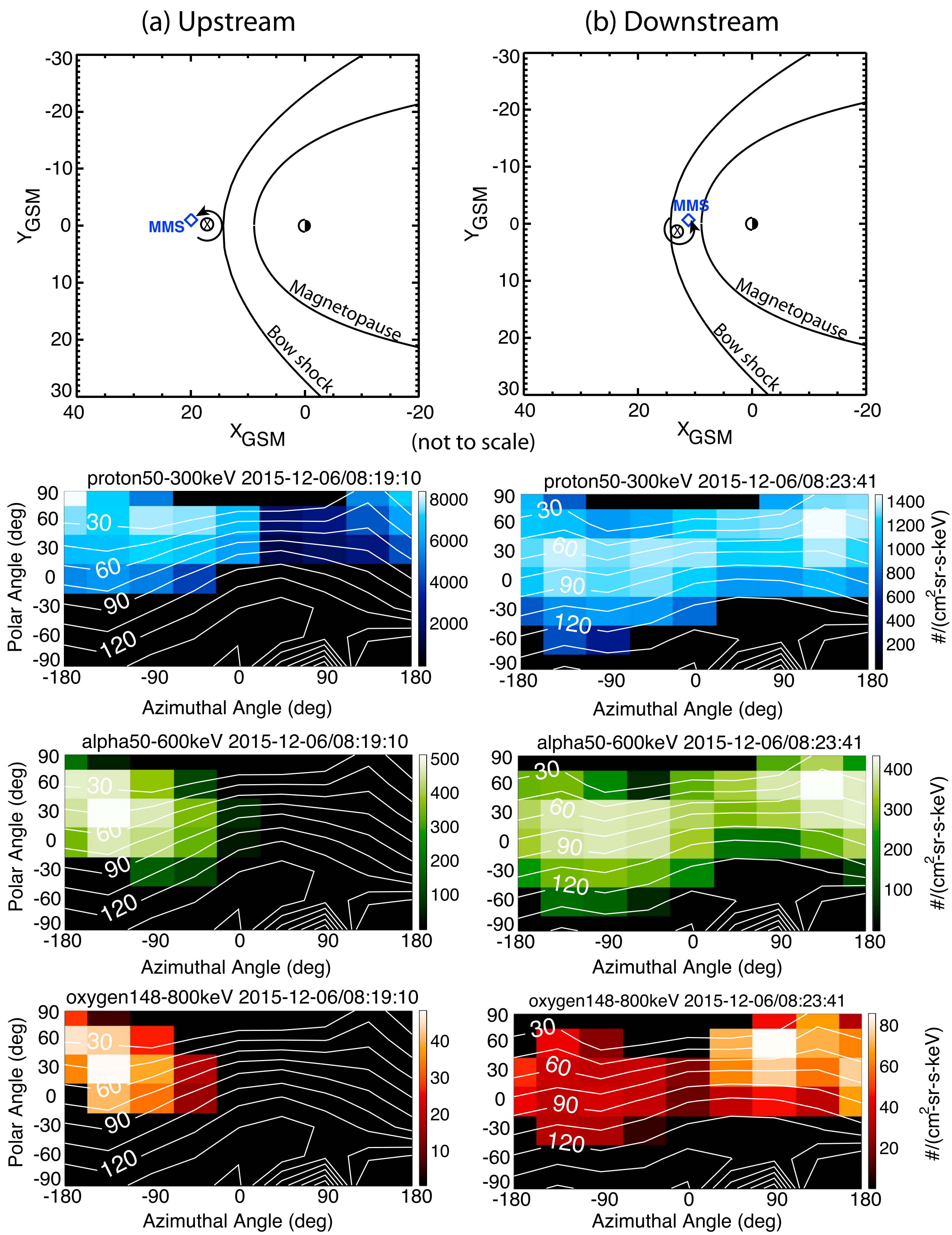

Figure 2. (first row) A schematic sketch of the particle trajectories in the (a) upstream and (b) downstream from the bow shock. (second to fourth rows) Energetic proton (blue), helium (green), and oxygen (red) ion angular distributions (polar versus azimuthal angle) measured at 08:19:10–08:19:30 UT (Figure 2a) and at 08:23:41–08:24:00 UT (Figure 2b). The white lines depict contours of constant pitch angles.

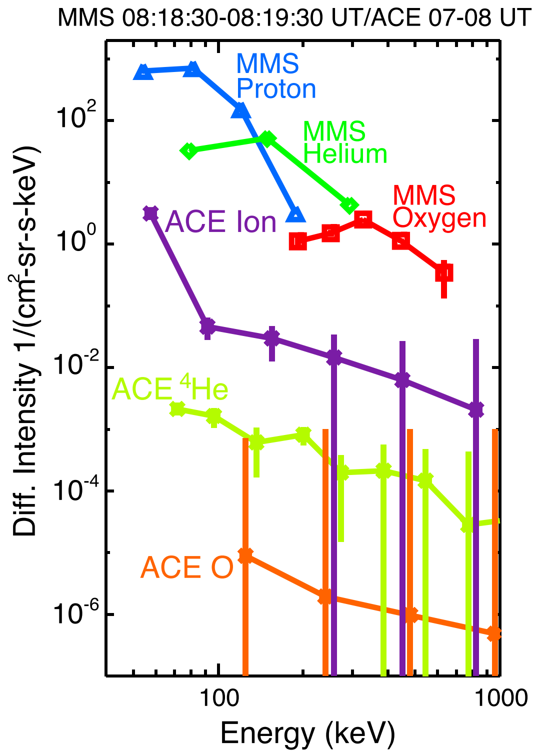

Figure 3. Comparison of time-averaged MMS (1 min) and ACE (1 h) ion energy spectra. Error bars are standard deviations for each subinterval.

connected to the bow shock. Perhaps they were also accelerated by Fermi acceleration process at the bow shock.

Magnetospheric energetic ions are often present in the quasi-parallel region of the bow shock when the IMF connects to the bow shock. These ions can stream along the magnetosheath magnetic field and further escape into the upstream region of the bow shock [e.g., *Sarris et al.*, 1976; *Krimigis et al.*, 1978; *Luhmann et al.*, 1984; *Krimigis et al.*, 1986; *Anagnostopoulos et al.*, 1986]. The IMF orientation changes from a quasi-parallel to a quasi-perpendicular direction at 08:18:10 UT (Figure 1r). The magnetospheric ions cannot escape directly into the region upstream from the quasi-perpendicular bow shock since the IMF does not connect to the bow shock. However, the energetic ions continue to appear in the quasi-perpendicular region of the bow shock and the inverse dispersions are observed in all three ion species from 08:18:10 UT to 08:19:30 UT.

3.2. How Do the Magnetospheric Ions Reach the Quasi-Perpendicular Bow Shock?

In this section, we will describe how energetic ions can escape from the magnetosphere through the magnetosheath and into the quasi-parallel foreshock, perhaps becoming energized by Fermi acceleration, and subsequently find themselves on magnetic field lines that do not connect to the magnetosphere and be present in the region upstream from the quasi-perpendicular bow shock. We invoke gradient drift, which is one possibility, to explain how this could happen.

The quasi-parallel foreshock is full of particles. Reflected or counterstreaming ions (∼10–40 keV) and diffuse ions (∼30–100 keV) are the two distinct populations of backward streaming energetic ions in the foreshock region [*Gosling et al.*, 1978]. Diffuse ions have relatively broad velocity distributions extending to considerably higher energies and are associated with large-amplitude magnetic and density fluctuations. The wave-particle scattering between the upstream and downstream waves provides first-order Fermi acceleration process and leads to diffuse ion populations upstream from quasi-parallel shocks [*Lee*, 1982]. Thus, the diffuse ions are commonly observed both upstream and downstream from the quasi-parallel bow shock [*Gosling et al.*, 1978; *Paschmann et al.*, 1981].

Kis et al. [2004] demonstrated that the spatial gradient of the partial density of upstream diffuse ions (∼10 keV to ∼32 keV) decreased exponentially with an *e*-folding distance from the shock front. The *e*-folding distance depends on the particle energy. Similar results were reported by *Ipavich et al.* [1981a]; *Trattner et al.* [1994]; *Kronberg et al.* [2009]; *Trattner et al.* [2013].

Sibeck et al. [2001] presented case and statistical surveys of foreshock events using the IMP 8 observations, showing that energetic ions can enhance the total pressure and depress the foreshock magnetic field strength and density within bundles of magnetic field lines connected to the bow shock. As the cavities expand, the excavated plasma and magnetic fields pile up on the boundaries. Foreshock magnetic field strengths and densities can increase by a factor of ∼2 when energetic ion bursts are present in the foreshock regions. Therefore, at the edges of the foreshock, i.e., at the boundary between the foreshock and the quasi-perpendicular regions upstream from the bow shock, there are positive gradients in the magnetic field strength in two directions: (1) from the quasi-parallel foreshock toward the enhanced fields that bound the

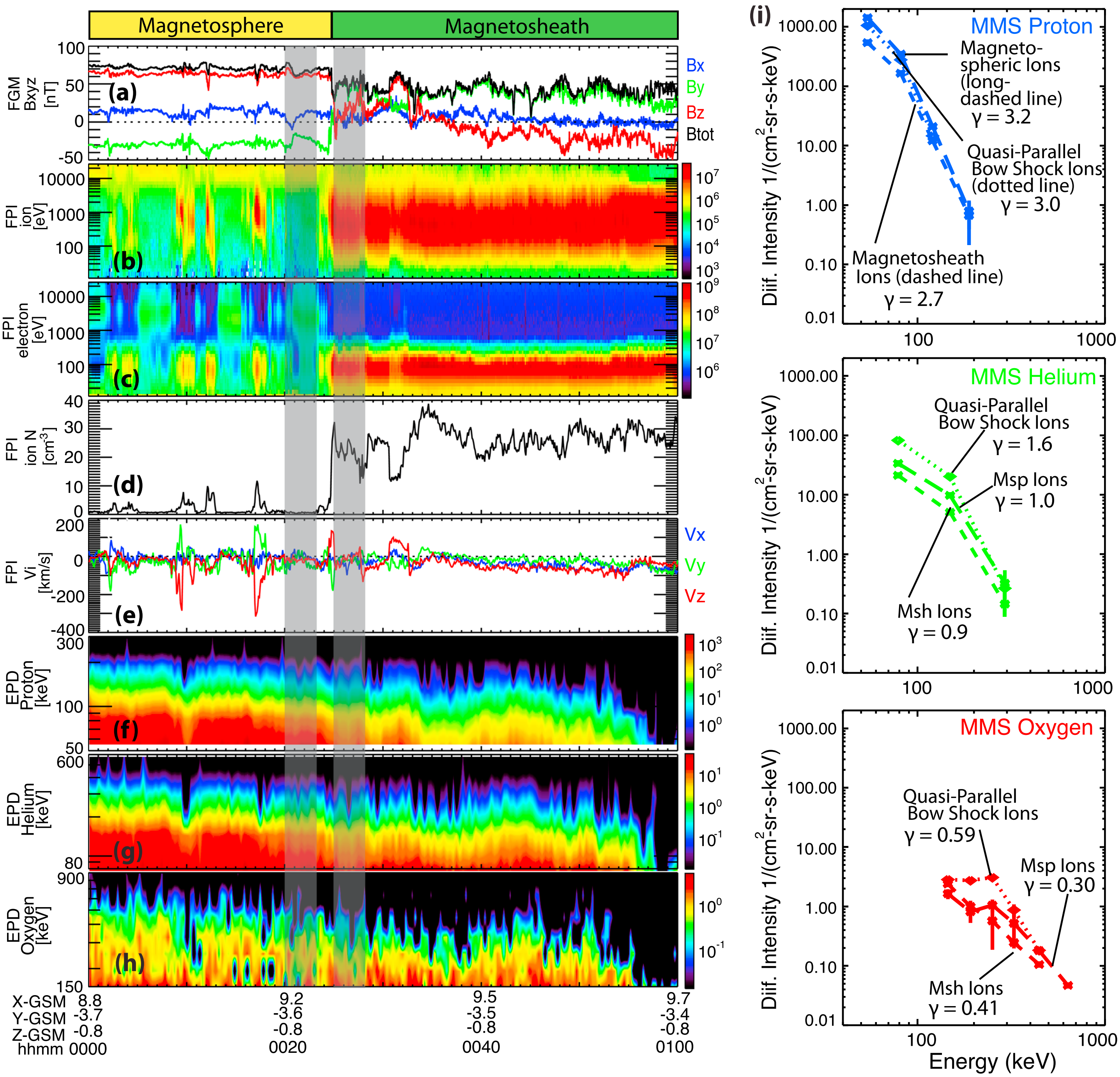

Figure 4. Magnetosphere data from 00:00 to 01:00 UT on 6 December 2015. (a) The three components of the magnetic field in GSM coordinates and the total magnetic field strength; (b) ion energy spectrum; (c) electron energy spectrum; (d) ion density; (e) the three components of the ion flow velocity; and energetic (f) proton, (g) helium, and (h) oxygen ion energy spectrum. (i) Comparison of energy spectra detected between 00:20 and 00:23 UT (long-dashed line), between 00:25 and 00:28 UT (dashed line), and between 08:17:20 and 08:18:20 UT (dotted line).

quasi-perpendicular bow shock and (2) from the bow shock outward into the solar wind along the regions of enhanced fields that bound the foreshock.

Figure 5 illustrates how magnetospheric ions (possibly accelerated) within the foreshock region upstream from the quasi-parallel bow shock might gradient drift across the foreshock boundary region of enhanced magnetic field strengths. They would then be convected into the region upstream from the quasi-perpendicular bow shock and perhaps further energized by shock drift acceleration. The gyroradius of

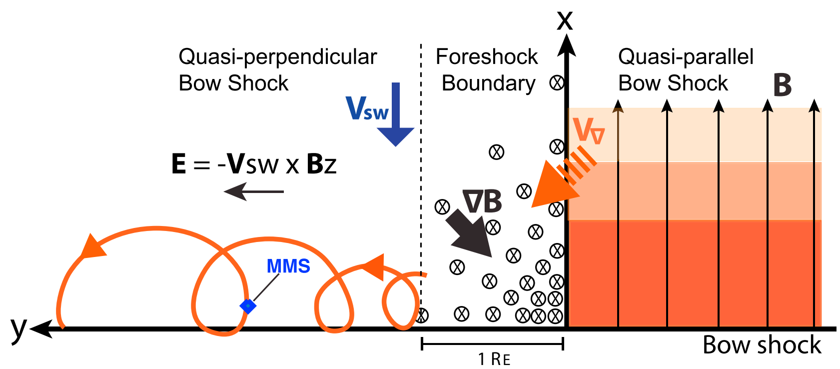

Figure 5. A schematic sketch of the shock geometry relating how the energetic ions reach the quasi-perpendicular region of the bow shock. Magnetospheric ions Fermi accelerated within the foreshock upstream from the quasi-parallel bow shock might gradient drift across the edges of the foreshock and then would be convected into the bow shock where further shock drift acceleration may occur. The gyroradius of the convected energetic ion would be increased by the electric field during the gradient drift in the region upstream from the quasi-perpendicular bow shock. The sequence of events enables spacecraft upstream from the quasi-perpendicular bow shock to observe ions escaping from the magnetosphere.

the convected energetic ion in the upstream from the quasi-perpendicular bow shock would be increased by the electric field during the gradient drift which will be discussed in the next section in more detail (Figure 7). Here the bow shock lies within the Y-Z plane at $X = 0$, and the solar wind is at $X > 0$. The quasi-parallel foreshock lies at $Y < 0$, the foreshock boundary with a dawnward and earthward gradient in enhanced magnetic field strengths is at $0 < Y < 1\ R_E$, and the quasi-perpendicular region of the bow shock is at $Y > 1$.

Shading in Figure 5 indicates flux levels of energetic ions in the regions upstream from the bow shock. Fluxes are large immediately upstream from the quasi-parallel bow shock but are known from past work to decrease with distance from the bow shock. There are no fluxes of energetic ions far upstream. The suprathermal particles exert additional pressure that causes an expansion of the region of the quasi-parallel foreshock due to the diamagnetic effect. As it expands, the foreshock compresses adjacent regions in which the IMF does not connect to the bow shock [*Sibeck et al.*, 2001, 2008]. Consequently, there are gradients (∇B) in the foreshock compressional boundary region of magnetic field lines not connected to the bow shock. These gradients point toward the foreshock and bow shock. Energetic ions may undergo gradient drifts ($\mathbf{V}_\nabla$) from the foreshock toward the quasi-perpendicular bow shock region. We made a calculation according to this scenario.

Consistent with observations, we consider a large-amplitude magnetic field strength variation ($\delta B/B \approx 0.75$) at the foreshock boundary [*Paschmann et al.*, 1979; *Sibeck et al.*, 1989; *Fairfield et al.*, 1990]. The gradient in the magnetic field strength is not clearly visible in Figure 1m; however, there is a magnetic field bump ($B \approx 14$ nT) at 08:18:10 UT (at the edge of the foreshock). Then we assume that the magnetic field strength is given by

$$\mathbf{B} = B_0 + B_1 \exp\left[-k_x \mathbf{x}\right] \exp\left[-k_y \mathbf{y}\right] , \tag{1}$$

where B_0 (8 nT) and B_1 (6 nT) are the background and perturbation magnetic field strengths and k_x ($= 2\pi/\lambda_x$) and k_y ($= 2\pi/\lambda_y$) are the wave number for perturbation to decay from the front of the bow shock in the X and Y directions, respectively. We chose wavelengths λ_x (λ_y) ranging from 1 R_E to 5 R_E, consistent with dimensions for foreshock boundaries derived from previous observational studies [e.g., *Fairfield et al.*, 1990]. We take the gradient of the magnetic field ∇B and estimate the gradient magnetic field drift velocity. This gives

$$\mathbf{V}_\nabla = \frac{mv^2}{2q}\left(\frac{\mathbf{B}\times\nabla B}{B^3}\right) = \frac{mv^2}{2q}\,\frac{\left(B_z(\nabla_x B)\mathbf{y} - B_z(\nabla_y B)\mathbf{x}\right)}{B^3} , \tag{2}$$

where $mv^2/2$ is the energy of the particles and q is the ion charge. The gradient magnetic field drift is perpendicular to the magnetic field ($\mathbf{B}$) and the gradient B (∇B). B_z is the dominant component of the magnetic field in the quasi-perpendicular bow shock in our case ($B_z \approx B \approx 10$ nT). The X component of the magnetic field (~7 nT) dominates in the quasi-parallel foreshock.

We wish to determine how quickly energetic ions can drift out of the quasi-parallel foreshock into the regions of enhanced magnetic field strengths that bound the foreshock to see whether a layer or region of escaping

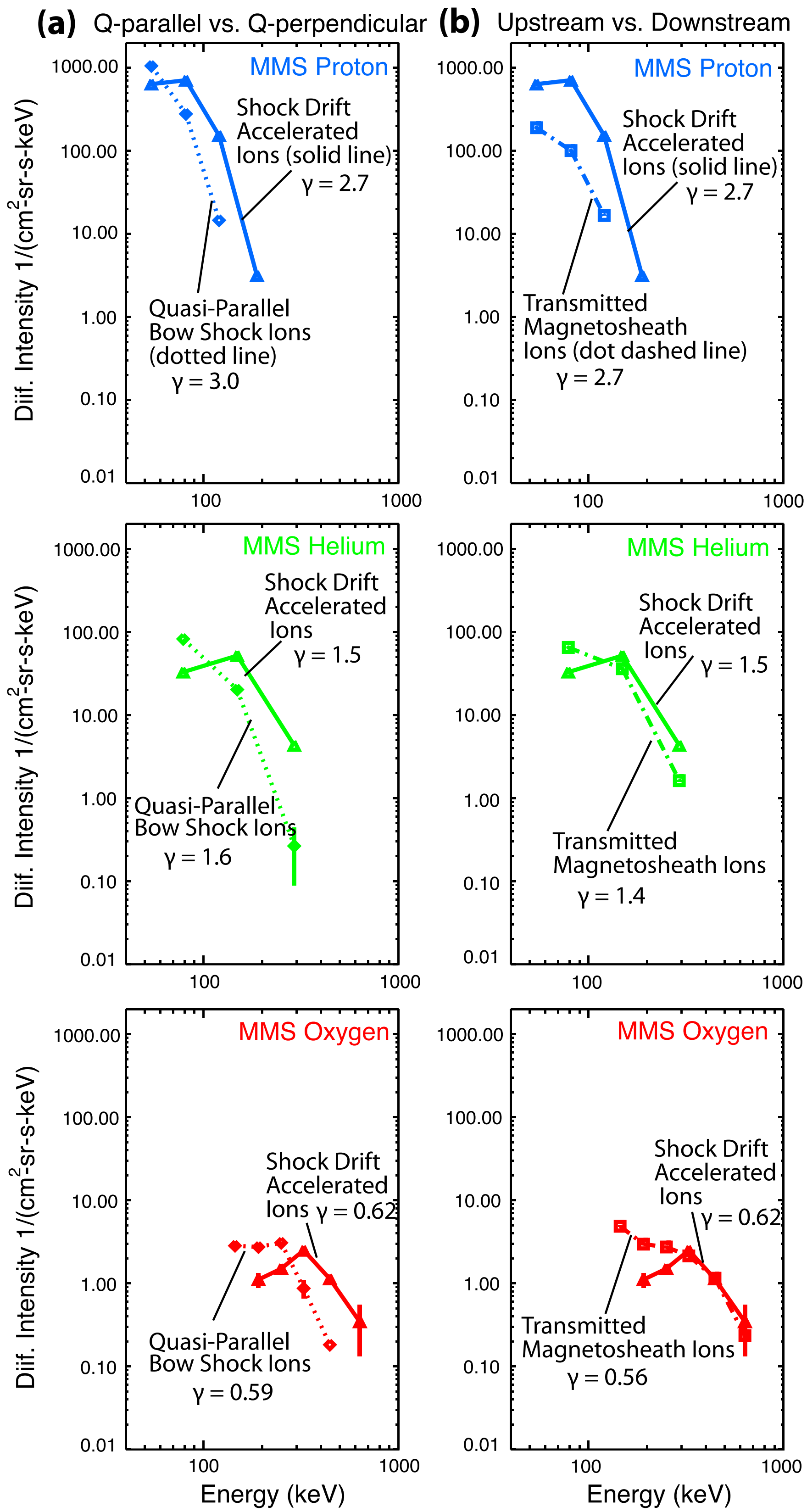

Figure 6. A comparison of energetic ion energy spectra (a) in the region upstream from the quasi-parallel (dotted lines) and quasi-perpendicular bow shock (solid lines), (b) in the region downstream of the bow shock (dash-dotted lines).

magnetospheric ions can appear within the quasi-perpendicular foreshock on the edge of the quasi-parallel foreshock. Examples of the calculated drift velocities ($\mathbf{V}_\nabla$) for a wavelength of λ_x (λ_y) = 1 R_E (a scale for the magnetic field gradient) are about 5.0×10^3 km/s for protons with energy of 60 keV, 4.2×10^3 km/s for helium ions with energy of 100 keV and 17×10^3 km/s for oxygen ions with energy of 200 keV. The drift is very rapid; thus, the region adjacent to the foreshock could be immediately filled with the energetic ions drifting out of the quasi-parallel foreshock.

Our observations indicate that the duration of the inverse dispersion is about 1 min. The solar wind ($V_{sw} \approx 400$ km/s) can move ~4 R_E during that minute. However, it only requires ~5 s for protons drifting 5.0×10^3 km/s to fill up the quasi-perpendicular region to a distance of ~4 R_E. The drifting energetic ions are then convected with the solar wind moving toward the shock front. Consequently, the convected energetic ions may still be seen upstream from the quasi-perpendicular bow shock for 1/,min.

The gyroradii for 60 keV protons (H^+), 100 keV helium (He^{2+}), and 200 keV oxygen (O^+) ions in a 10 nT field are about 0.5, 1.0, and 4.0 R_E, respectively. The gyroradii for the protons and helium ions are smaller than ~4 R_E, which is the approximate depth that the ions were seen into the quasi-perpendicular region; the escape out of the foreshock by finite gyroradius effects can be ruled out as a possible explanation for the energetic ions upstream from the quasi-perpendicular bow shock.

The convected quasi-parallel bow shock ions can be further energized by shock drift acceleration process in the quasi-perpendicular bow shock region. Figure 6a shows a comparison between the ion intensities for each species at the quasi-parallel bow shock region from 08:17:20 UT to 08:18:20 UT (dotted lines) and quasi-perpendicular bow shock region from 08:18:30 UT to 08:19:30 UT (solid lines). The two time intervals selected are marked by gray and blue shaded regions in Figures 1m–1v, and the energy spectra are about 1 min averaged. There is a hump in the flux at the middle energy channels and flux enhancements at higher energies, indicating further energization by shock drift acceleration. Energization via the shock drift acceleration can be estimated by comparing the energies of ions observed in the quasi-parallel bow shock (possibly accelerated by Fermi acceleration process) and in the quasi-perpendicular bow shock (shock drift acceleration). The characteristic energies of the proton, helium, and oxygen ions approximately increase by about a factor of 2 possibly through shock drift acceleration process.

3.3. What Causes the Inverse Dispersions of Energetic Ions in the Region Upstream and in the Magnetosheath?

Bursts of energetic ions (~50 keV to 1 MeV) exhibiting inverse energy dispersions were observed in the regions upstream and downstream from the bow shock. In this section, we compare the characteristics of our inverse dispersion events with those in previous studies and investigate a possible mechanism to produce the observed inverse dispersions.

Inverse dispersed ion signatures observed in the region upstream and outer magnetosphere have been previously reported [e.g., *Ipavich et al.*, 1981a]. *Ipavich et al.* [1981a] reported inverse velocity dispersions in 33 upstream particle events in the energy range from ~30 keV/Q to ~130 keV/Q (protons). The lower energy particles first reach their maximum intensities (plateau) about ~15 min to ~2 h before the higher energy plateau appears. *Ipavich et al.* [1981a] interpreted the inverse dispersion patterns within the Fermi acceleration model that describes the relationship between the acceleration time and the particle energies. The higher energy particles require more time to reach their equilibrium intensities since the diffusion coefficient linearly depends on energy.

Anagnostopoulos et al. [1998] reported that 18% of the upstream energetic (≥50 keV) ion events (total 125 events) showed inverse energy dispersion patterns. *Anagnostopoulos et al.* [1998] suggested that both (1) leakage and (2) diffusive acceleration models can predict the inverse dispersions. (1) If the IMF connects to the bow shock (quasi-parallel bow shock), high-energy magnetospheric ions can escape into the region upstream from the bow shock. Inverse dispersions can be expected in the upstream region when the high-energy magnetospheric energetic ions are injected from the inner magnetosphere under a preexisting stable low-energy ion flux condition. (2) The Fermi acceleration model predicts that the inverse dispersion can be observed in the upstream region since the acceleration process depends on time and is associated with an energy-dependent time constant. The lowest limit of the time duration of the inverse dispersion events is about 15 min.

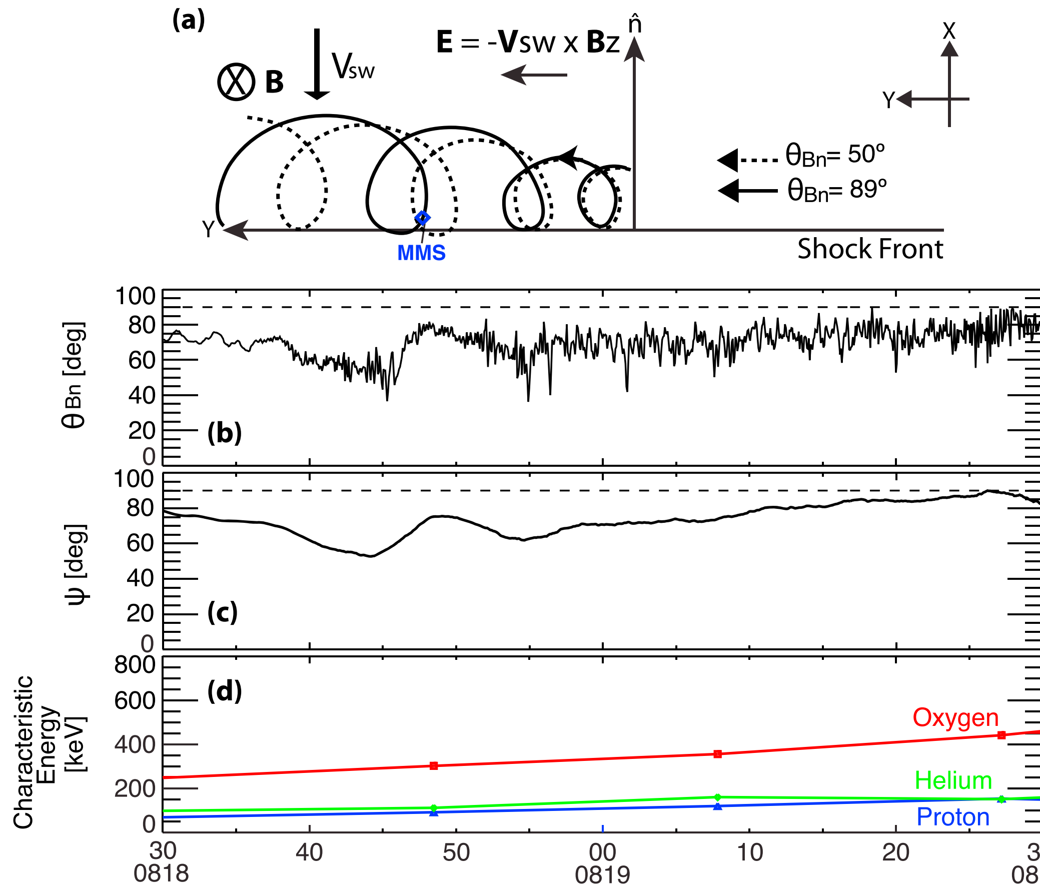

Figure 7. (a) Projections of the motion of the energetic ions into the *X*-*Y* plane with the two different magnitudes of the electric field according to the two θ_{Bn} angles marked by two arrows. (b) θ_{Bn} (angle between magnetic field and local bow shock normal), (c) ψ (angle between the magnetic field and solar wind velocity), and (d) kinetic energies of the energetic ions in the inverse dispersion from 08:18:30 UT to 08:19:30 UT.

There are differences between the inverse dispersion events observed by MMS and those reported by *Ipavich et al.* [1981a] and *Anagnostopoulos et al.* [1998]: (1) Our inverse dispersions were observed in the vicinity of the quasi-perpendicular and nearly perpendicular bow shock. Thus, they cannot be explained solely by the leakage and/or Fermi acceleration models that operate at the quasi-parallel bow shock. (2) The whole process of the inverse dispersion events is completed in several minutes (~1–3 min).

Instead, we suggest that the inverse dispersions result from shock drift acceleration when the geometry changes from a quasi-perpendicular to a nearly perpendicular bow shock configuration with a larger θ_{Bn} angle ($\theta_{Bn} \approx 90°$). Shock drift acceleration models predict maximum efficiency energizing particles when the IMF lies nearly tangential to the bow shock front [*Anagnostopoulos and Sarris*, 1983]. Particles can gain energy by gradient drifting through the induced interplanetary electric field, $|\mathbf{E}| = -|\mathbf{V}_{SW} \times \mathbf{B}| = -V_{SW} B \sin\psi$, where ψ is the angle between the magnetic field $\mathbf{B}$ and the solar wind velocity $\mathbf{V}_{SW}$. The magnitude of the electric field increases with larger angles ψ, which is similar to the angle θ_{Bn} if $\mathbf{V}_{SW}$ and $\hat{n}$ (the local shock normal) lie nearly along the *X* axis. Larger angles θ_{Bn} (or $\psi \approx 90°$) also allow the direction of the induced electric field to be parallel to the bow shock front, and then particles can drift for a longer distance along the electric field. Thus, particles can achieve more energy.

Figure 7a shows schematic trajectories for the reflected energetic ions in the quasi-perpendicular (the dashed curve) and nearly perpendicular (the solid curve) shock geometries projected onto the *X*-*Y* plane. The θ_{Bn} angles for the two cases of the particle motion differ. Two ions begin gradient drifting along the bow shock in the positive *Y* direction from a starting point at $Y = 0$ due to the presence of a southward IMF and a strong gradient in the magnetic field strength at the bow shock in the negative *X* direction. The ions drift in the direction of the convection electric field, so they gain energy. The gyroradii of both cases should begin the same and gradually increase with time or distance along the positive Y axis. However, the electric field is larger for one case than the other, and therefore this ion will gain more energy than the other by the time it reaches an observing spacecraft at large positive Y. A possible energy gain by drifting for a distance of 5 R_E parallel to the $\mathbf{V}_{SW} \times \mathbf{B}$ electric field, where $V_{SW} \approx 500$ km/s and $B \approx 10$ nT, is about 100 keV.

Matsukiyo et al. [2011] presented simulation runs for four different θ_{Bn} (60°, 80°, 85°, and 87°), showing that the most efficient electron shock drift acceleration (SDA) occurs for the largest θ_{Bn} (87°). *Gargaté and Spitkovsky* [2012] examined the effect of the shock parameters (Alfvén Mach number and θ_{Bn}) on the particle acceleration efficiency using hybrid and particle-in-cell (PIC) shock simulations. They found that particles are most efficiently accelerated to the higher energies at a large θ_{Bn} (~90°) in the quasi-perpendicular regime since the upstream electric field intensity is higher for larger θ_{Bn} angles.

There is a clear relationship between energetic ion flux and angles θ_{Bn} and ψ, and it is in the sense predicted by shock drift theory. Figures 7b–7d show from top to bottom the observed θ_{Bn}, ψ, and the characteristic energies of protons (blue), helium (green) and oxygen (red) ions, respectively, in the region upstream from the quasi-perpendicular bow shock from 08:18:30 UT to 08:19:30 UT (1 min). The angles θ_{Bn} and ψ gradually increase from ~50° at 08:18:45 UT to nearly 90° at 08:19:30 UT. Meanwhile, the characteristic energies of the protons increase from ~60 keV to ~150 keV, the helium ions from ~90 keV to ~170 keV, and the oxygen ions from ~250 keV to ~450 keV. This indicates that the angle θ_{Bn} and the ion energies are closely related.

About 3 min after the upstream inverse dispersions, another inverse dispersion event was observed, this time in the magnetosheath, and the events are very similar. Figure 6b compares the energetic ion spectra in the region upstream from the quasi-perpendicular bow shock (solid lines) with those downstream from the bow shock (dash-dotted lines). The comparison indicates similar helium and oxygen ion flux levels but lower proton flux level in the magnetosheath inverse dispersions (dash-dotted lines) than that in the upstream inverse dispersions (solid lines). The spectral indices (γ) are also very similar. We suggest that the two inverse energy dispersions have similar origins. As θ_{Bn} increased, the energies of the ions increased and the energetic ions were swept downstream of the bow shock.

4. Summary and Conclusions

Bursts of energetic (~50 keV$\leq E \leq$1 MeV) proton, helium, and oxygen ions were observed by the MMS-EIS instrument upstream and downstream from the bow shock during the interval from 07:50 UT to 08:30 UT on 6 December 2015. All three ion species exhibited inverse energy dispersions, with the lower energy ions arriving first in the region upstream from the quasi-perpendicular bow shock (08:18:30 UT–08:19:30 UT) and in the magnetosheath (08:23:00 UT–08:25:00 UT). Analyzing the characteristics of the observed inverse dispersion of the energetic ions, the results can be summarized as follows:

1. The composition, flux level, and spectral slopes of the proton, helium, and oxygen ions observed by MMS upstream from the bow shock greatly resemble those observed in the outer magnetosphere and inner magnetosheath but differ greatly from those simultaneously seen in the upstream solar wind by ACE. This suggests that the energetic ions observed in the upstream and downstream region of the bow shock originated in the magnetosphere.
2. Energetic ions of magnetospheric origin were continuously observed in the region upstream from the quasi-perpendicular bow shock in which the IMF was disconnected to the magnetosphere. We suggest that the ions gradient drifted out of the nearby quasi-parallel foreshock and into the quasi-perpendicular region of the bow shock.
3. Each of the ion species exhibited an inverse dispersion. As predicted by models for shock drift acceleration, the energies of the ions increased as θ_{Bn}, the angle between the IMF and the shock normal, increased from ~50° to ~90°. The inverse dispersions can be caused by the IMF orientation changes, from quasi-perpendicular to (nearly) perpendicular local bow shock.
4. The characteristics (the composition, flux level, and spectral slope) of the inverse dispersion signatures observed in the subsolar magnetosheath were similar to those seen in the region upstream of the bow shock. We conclude that particles escape from the magnetosphere, find their way upstream, and further energize by shock drift acceleration at the bow shock. Then they are swept downstream of the bow shock.

Acknowledgments
We would like to thank the FGM, FPI, and EPD instrument teams of the MMS mission and EPAM and ULEIS instrument teams of the ACE mission for the successful spacecraft operation and for providing plasma and magnetic field data. We acknowledge that the MMS data were obtained from https://lasp.colorado.edu/mms/sdc/public/; the ACE data were obtained from http://www.srl.caltech.edu/ACE/ASC/level2/index.html. This research was supported by an appointment to the NASA Postdoctoral Program at the NASA/GSFC, administered by Universities Space Research Association through a contract with NASA. Some of the work conducted at NASA/GSFC was supported by the MMS project.

References

Anagnostopoulos, G. C., and E. T. Sarris (1983), Dominant acceleration processes of ambient energetic protons (E greater than or equal to 50 keV) at the bow shock conditions and limitations, *Planet. Space Sci.*, *31*, 689–699, doi:10.1016/0032-0633(83)90010-7.

Anagnostopoulos, G. C., E. T. Sarris, and S. M. Krimigis (1986), Magnetospheric origin of energetic ($E > 50$ keV) ions upstream of the bow shock: The October 31, 1977, event, *J. Geophys. Res.*, *91*, 3020–3028.

Anagnostopoulos, G. C., A. G. Rigas, E. T. Sarris, and S. M. Krimigis (1998), Characteristics of upstream energetic ($E \geq 50$ keV) ion events during intense geomagnetic activity, *J. Geophys. Res.*, *103*, 9521–9534, doi:10.1029/97JA02925.

Anagnostopoulos, G. C., N. Paschalidis, and A. N. Littas (2000), Energy time dispersion of a new class of magnetospheric ion events observed near the Earth's bow shock, *Ann. Geophys.*, *18*, 28–41, doi:10.1007/s00585-000-0028-8.

Anderson, K. A., R. P. Lin, F. Martel, C. S. Lin, G. K. Parks, and H. Reme (1979), Thin sheets of energetic electrons upstream from the Earth's bow shock, *Geophys. Res. Lett.*, *6*, 401–404, doi:10.1029/GL006i005p00401.

Armstrong, T. P., M. E. Pesses, and R. B. Decker (1985), Shock drift acceleration, in *Collisionless Shocks in the Heliosphere: A Tutorial Review*, vol. 35, edited by B. T. Tsurutani and R. G. Stone, pp. 271–285, AGU, Washington, D. C.

Asbridge, J. R., S. J. Bame, and I. B. Strong (1968), Outward flow of protons from the Earth's bow shock, *J. Geophys. Res.*, *73*, 5777–5782, doi:10.1029/JA073i017p05777.

Bieber, J. W., and E. C. Stone (1982), Energetic electrons in the magnetosheath and upstream of the bow shock, *J. Geophys. Res.*, *87*, 85–94, doi:10.1029/JA087iA01p00085.

Burch, J. L., T. E. Moore, R. B. Torbert, and B. L. Giles (2016), Magnetospheric multiscale overview and science objectives, *Space Sci. Rev.*, *199*, 5–21, doi:10.1007/s11214-015-0164-9.

Burgess, D. (1987), Shock drift acceleration at low energies, *J. Geophys. Res.*, *92*, 1119–1130, doi:10.1029/JA092iA02p01119.

Cohen, I. J., et al. (2016), Observations of energetic particle escape at the magnetopause: Early results from the MMS Energetic Ion Spectrometer (EIS), *Geophys. Res. Lett.*, *43*, 5960–5968, doi:10.1002/2016GL068689.

Decker, R. B. (1983), Formation of shock-spike events at quasi-perpendicular shocks, *J. Geophys. Res.*, *88*, 9959–9973, doi:10.1029/JA088iA12p09959.

Decker, R. B. (1988), Computer modeling of test particle acceleration at oblique shocks, *Space Sci. Rev.*, *48*, 195–262, doi:10.1007/BF00226009.

Eichler, D. (1981), Energetic particle spectra in finite shocks—The Earth's bow shock, *Astrophys. J.*, *244*, 711–716, doi:10.1086/158748.

Ellison, D. C. (1985), Shock acceleration of diffuse ions at the Earth's bow shock: Acceleration efficiency and *A/Z* enhancement, *J. Geophys. Res.*, *90*, 29–38, doi:10.1029/JA090iA01p00029.

Ellison, D. C., and E. Moebius (1987), Diffusive shock acceleration—Comparison of a unified shock model to bow shock observations, *Astrophys. J.*, *318*, 474–484, doi:10.1086/165384.

Ellison, D. C., and R. Ramaty (1985), Shock acceleration of electrons and ions in solar flares, *Astrophys. J.*, *298*, 400–408, doi:10.1086/163623.

Fairfield, D. H., W. Baumjohann, G. Paschmann, H. Luehr, and D. G. Sibeck (1990), Upstream pressure variations associated with the bow shock and their effects on the magnetosphere, *J. Geophys. Res.*, *95*, 3773–3786.

Gargaté, L., and A. Spitkovsky (2012), Ion acceleration in non-relativistic astrophysical shocks, *Astrophys. J.*, *744*, 67, doi:10.1088/0004-637X/744/1/67.

Giacalone, J. (2004), Large-scale hybrid simulations of particle acceleration at a parallel shock, *Astrophys. J.*, *609*, 452–458, doi:10.1086/421043.

Gold, R. E., S. M. Krimigis, S. E. Hawkins, D. K. Haggerty III, D. A. Lohr, E. Fiore, T. P. Armstrong, G. Holland, and L. J. Lanzerotti (1998), Electron, proton, and alpha monitor on the Advanced Composition Explorer spacecraft, *Space Sci. Rev.*, *86*, 541–562, doi:10.1023/A:1005088115759.

Gosling, J. T., J. R. Asbridge, S. J. Bame, G. Paschmann, and N. Sckopke (1978), Observations of two distinct populations of bow shock ions in the upstream solar wind, *Geophys. Res. Lett.*, *5*, 957–960, doi:10.1029/GL005i011p00957.

Greenstadt, E. W., G. Le, and R. J. Strangeway (1995), ULF waves in the foreshock, *Adv. Space Res.*, *15*, 71–84, doi:10.1016/0273-1177(94)00087-H.

Ipavich, F. M., A. B. Galvin, G. Gloeckler, M. Scholer, and D. Hovestadt (1981a), A statistical survey of ions observed upstream of the Earth's bow shock—Energy spectra, composition, and spatial variation, *J. Geophys. Res.*, *86*, 4337–4342, doi:10.1029/JA086iA06p04337.

Ipavich, F. M., G. Gloeckler, and M. Scholer (1981b), Temporal development of composition, spectra, and anisotropies during upstream particle events, *J. Geophys. Res.*, *86*, 11,153–11,160, doi:10.1029/JA086iA13p11153.

Kahler, S. (1994), Injection profiles of solar energetic particles as functions of coronal mass ejection heights, *Astron. Astrophys.*, *428*, 837–842, doi:10.1086/174292.

Kis, A., M. Scholer, B. Klecker, E. Möbius, E. A. Lucek, H. Rème, J. M. Bosqued, L. M. Kistler, and H. Kucharek (2004), Multi-spacecraft observations of diffuse ions upstream of Earth's bow shock, *Geophys. Res. Lett.*, *31*, L20801, doi:10.1029/2004GL020759.

Krimigis, S. M., D. Venkatesan, J. C. Barichello, and E. T. Sarris (1978), Simultaneous measurements of energetic protons and electrons in the distant magnetosheath, magnetotail, and upstream in the solar wind, *Geophys. Res. Lett.*, *5*, 961–964, doi:10.1029/GL005i011p00961.

Krimigis, S. M., D. G. Sibeck, and R. W. McEntire (1986), Magnetospheric particle injection and the upstream ion event of September 5, 1984, *Geophys. Res. Lett.*, *13*, 1376–1379.

Kronberg, E. A., A. Kis, B. Klecker, P. W. Daly, and E. A. Lucek (2009), Multipoint observations of ions in the 30–160 keV energy range upstream of the Earth's bow shock, *J. Geophys. Res.*, *114*, A03211, doi:10.1029/2008JA013754.

Lee, M. A. (1982), Coupled hydromagnetic wave excitation and ion acceleration upstream of the Earth's bow shock, *J. Geophys. Res.*, *87*, 5063–5080.

Lee, S. H., et al. (2016), Inverse energy dispersion of energetic ions observed in the magnetosheath, *Geophys. Res. Lett.*, *43*, 7338–7347, doi:10.1002/2016GL069840.

Lin, R. P., C.-I. Meng, and K. A. Anderson (1974), 30- to 100-keV protons upstream from the Earth's bow shock, *J. Geophys. Res.*, *79*, 489–498, doi:10.1029/JA079i004p00489.

Louarn, P., et al. (2003), Observation of energy-time dispersed ion structures in the magnetosheath by CLUSTER: Possible signatures of transient acceleration processes at shock, *Ann. Geophys.*, *21*, 1483–1495, doi:10.5194/angeo-21-1483-2003.

Luhmann, J. G., R. J. Walker, C. T. Russell, N. U. Crooker, J. R. Spreiter, and S. S. Stahara (1984), Patterns of potential magnetic field merging sites on the dayside magnetopause, *J. Geophys. Res.*, *89*, 1739–1745.

Mason, G. M., et al. (1998), The Ultra-Low-Energy Isotope Spectrometer (ULEIS) for the ACE spacecraft, *Space Sci. Rev.*, *86*, 409–448, doi:10.1023/A:1005079930780.

Matsukiyo, S., Y. Ohira, R. Yamazaki, and T. Umeda (2011), Relativistic electron shock drift acceleration in low Mach number galaxy cluster shocks, *Astrophys. J.*, *742*, 47, doi:10.1088/0004-637X/742/1/47.

Mauk, B. H., et al. (2014), The Energetic Particle Detector (EPD) investigation and the Energetic Ion Spectrometer (EIS) for the Magnetospheric Multiscale (MMS) mission, *Space Sci. Rev.*, *199*, 471–514, doi:10.1007/s11214-014-0055-5.

Merka, J., A. Szabo, J. A. Slavin, and M. Peredo (2005), Three-dimensional position and shape of the bow shock and their variation with upstream Mach numbers and interplanetary magnetic field orientation, *J. Geophys. Res.*, *110*, A04202, doi:10.1029/2004JA010944.

Paschmann, G., N. Sckopke, I. Papamastorakis, J. R. Asbridge, S. J. Bame, and J. T. Gosling (1981), Characteristics of reflected and diffuse ions upstream from the Earth's bow shock, *J. Geophys. Res.*, *86*, 4355–4364, doi:10.1029/JA086iA06p04355.

Paschmann, G., I. Papamastorakis, N. Sckopke, G. Haerendel, B. U. Ö. Sonnerup, S. J. Bame, J. R. Asbridge, J. T. Gosling, C. T. Russel, and R. C. Elphic (1979), Plasma acceleration at the Earth's magnetopause: Evidence for reconnection, *Nature*, *282*, 243–246.

Pollock, C., et al. (2016), Fast plasma investigation for magnetospheric multiscale, *Space Sci. Rev.*, *199*, 331–406, doi:10.1007/s11214-016-0245-4.

Reames, D. V., J. P. Meyer, and T. T. von Rosenvinge (1994), Energetic-particle abundances in impulsive solar flare events, *Astrophys. J. Suppl. Ser.*, *90*, 649–667, doi:10.1086/191887.

Russell, C. T., et al. (2014), The magnetospheric multiscale magnetometers, *Space Sci. Rev.*, *199*, 189–256, doi:10.1007/s11214-014-0057-3.

Sarris, E. T., S. M. Krimigis, C. O. Bostrom, T. Iijima, and T. P. Armstrong (1976), Location of the source of magnetospheric energetic particle bursts by multispacecraft observations, *Geophys. Res. Lett.*, *3*, 437–440, doi:10.1029/GL003i008p00437.

Sarris, E. T., G. C. Anagnostopoulos, and S. M. Krimigis (1987), Simultaneous measurements of energetic ion (50 keV and above) and electron (220 keV and above) activity upstream of Earth's bow shock and inside the plasma sheet—Magnetospheric source for the November 3 and December 3, 1977 upstream events, *J. Geophys. Res.*, *92*, 12,083–12,096, doi:10.1029/JA092iA11p12083.

Scholer, M., D. Hovestadt, F. M. Ipavich, and G. Gloeckler (1980), Conditions for acceleration of energetic ions greater than 30 keV associated with the Earth's bow shock, *J. Geophys. Res.*, *85*, 4602–4606, doi:10.1029/JA085iA09p04602.

Scholer, M., K. J. Trattner, and H. Kucharek (1992), Ion injection and Fermi acceleration at earth's bow shock—The 1984 September 12 event revisited, *Astrophys. J.*, *395*, 675–681, doi:10.1086/171687.

Sibeck, D. G., R. W. McEntire, A. T. Y. Lui, R. E. Lopez, S. M. Krimigis, R. B. Decker, L. J. Zanetti, and T. A. Potemra (1987), Energetic magnetospheric ions at the dayside magnetopause: Leakage or merging?, *J. Geophys. Res.*, *92*, 12,097–12,114.

Sibeck, D. G., R. W. McEntire, S. M. Krimigis, and D. N. Baker (1988), The magnetosphere as a sufficient source for upstream ions on November 1, 1984, *J. Geophys. Res.*, *93*, 14,328–14,342.

Sibeck, D. G., W. Baumjohann, R. C. Elphic, D. H. Fairfield, and J. F. Fennell (1989), The magnetospheric response to 8-minute period strong-amplitude upstream pressure variations, *J. Geophys. Res.*, *94*, 2505–2519, doi:10.1029/JA094iA03p02505.

Sibeck, D. G., R. B. Decker, D. G. Mitchell, A. J. Lazarus, R. P. Lepping, and A. Szabo (2001), Solar wind preconditioning in the flank foreshock: IMP 8 observations, *J. Geophys. Res.*, *106*, 21,675–21,688, doi:10.1029/2000JA000417.

Sibeck, D. G., N. Omidi, I. Dandouras, and E. Lucek (2008), On the edge of the foreshock: Model-data comparisons, *Ann. Geophys.*, *26*, 1539–1544, doi:10.5194/angeo-26-1539-2008.

Terasawa, T. (1979), Origin of 30–100 keV protons observed in the upstream region of the Earth's bow shock, *Planet. Space Sci.*, *27*, 365–384, doi:10.1016/0032-0633(79)90114-4.

Torbert, R. B., et al. (2014), The FIELDS instrument suite on MMS: Scientific objectives, measurements, and data products, *Space Sci. Rev.*, *199*, 105–135, doi:10.1007/s11214-014-0109-8.

Trattner, K. J., E. Mobius, B. Klecker, M. Hilchenbach, and H. Luhr (1994), Statistical analysis of diffuse ion events upstream of the Earth's bow shock, *J. Geophys. Res.*, *99*, 13,389–13,400.

Trattner, K. J., et al. (2013), The free escape continuum of diffuse ions upstream of the Earth's quasi-parallel bow shock, *J. Geophys. Res. Space Physics*, *118*, 4425–4434, doi:10.1002/jgra.50447.

Zong, Q.-G., B. Wilken, S.-Y. Fu, T. A. Fritz, Z.-Y. Pu, N. Hasebe, and D. J. Williams (2001), Ring current oxygen ions in the magnetosheath caused by magnetic storm, *J. Geophys. Res.*, *106*, 25,541–25,556.